Supporting Information

Dioxolanone Anchored Poly (Allyl Ether)-Based Cross-Linked Dual-Salt Polymer Electrolytes for High-Voltage Lithium Metal Batteries

Vidyanand Vijayakumar,[#,$,&] Diddo Diddens,[#] Andreas Heuer, [#, £] Sreekumar Kurungot,[&,*] Martin Winter,[#, £,¥,*] Jijeesh Ravi Nair[#,*]

[#]Helmholtz Institute Münster, IEK-12, Forschungszentrum Jülich GmbH, Corrensstraße 46, 48149 Münster, Germany. E-mail: j.nair@fz-juelich.de (JRN), m.winter@fz-juelich.de (MW).

[$]Academy of Scientific and Innovative Research (AcSIR), Sector 19, Kamla Nehru Nagar, Ghaziabad, Uttar Pradesh- 201002, India.

[&]Physical and Materials Chemistry Division, CSIR-National Chemical Laboratory, Pune- 411008, India. E-mail: k.sreekumar@ncl.res.in (SK)

[£]Institute of Physical Chemistry, University of Münster, Corrensstraße 28/30, 48149, Münster, Germany. Email: Martin.Winter@uni-muenster.de (MW).

[¥]MEET Battery Research Center, Corrensstraße 46, 48149, Münster, Germany. Email: Martin.Winter@uni-muenster.de (MW).

Contents

SI Section 1: Experimental details

Sample name	molality of LiTFSI (m)	$[O]_{PEGDME}$/[Li] ratio
Li-P-1	0.93	24
Li-P-2	1.86	12
Li-P-3	2.8	8
Li-P-4	4.65	5
Li-P-5	7.3	3

Table S1 The formulation and $[O]_{PEGDME}$/[Li] ratios of all the LiTFSI/PEGDME (Li-P-x) bulk solutions.

Sample	No of moles of O from PEGDME $[O]_{PEGDME}$	No of moles of O from VEC $[O]_{VEC}$	No of moles of O from PEGDAE $[O]_{PEGDAE}$	No. of moles of Li^+-ions from LiTFSI [Li]	[O]*/[Li]
S-XPE-1	0.0085	0.006244	0.00445	0.00035	55
S-XPE-2	0.0070	0.006244	0.00445	0.00057	31
S-XPE-3	0.0059	0.006244	0.00445	0.000742	22
S-XPE-4	0.0046	0.006244	0.00445	0.000948	16
S-XPE-5	0.0034	0.006244	0.00445	0.0011	13

$[O]^* = [O]_{PEGDME} + [O]_{VEC} + [O]_{PEGDAE}$

Table S2 The formulation of the S-XPE-x reactive solutions and the related [O]/[Li] ratios.

Sample	No of moles of O from PEGDME $[O]_{PEGDME}$	No of moles of O from VEC $[O]_{VEC}$	No of moles of O from PEGDAE $[O]_{PEGDAE}$	No of moles of Li^+-ions from LITFSI &LiFSI [Li]	[O]*/[Li]
D-XPE-1	0.00825	0.00606	0.00432	0.0004924	38
D-XPE-2	0.00681	0.00606	0.00432	0.0007124	24
D-XPE-3	0.00577	0.00606	0.00432	0.0008724	18.5
D-XPE-4	0.00447	0.00606	0.00432	0.0010724	14
D-XPE-5	0.00333	0.00606	0.00432	0.0012434	11

$[O]^* = [O]_{PEGDME}+[O]_{VEC}+[O]_{PEGDAE}$

Table S3 Formulations of the D-XPE-x reactive solutions/D-XPEs and the related [O]/[Li] ratios.

Characterization methods and techniques

Differential scanning calorimetry (DSC) analysis is carried out using the Discovery DSC 2500, instrument (TA instruments). The sample preparation was carried out in a dry room to minimize moisture uptake and contamination. In a typical measurement, the samples were heated from 25 to 100°C and then cooled to −150°C, and then heated again up to 150 °C. The heating and cooling steps were carried out at a scan rate of 10°C min^{-1} under helium flux. From the DSC thermograms, the glass transition temperature (T_g) values of the respective specimens are extracted. Thermogravimetric analysis (TGA) was carried out using a Discovery TGA 5500 instrument that was additionally equipped with a Discovery Mass Spectrometer (MS). The test was carried out in the presence of helium carrier gas at a flow rate of 25 ml min^{-1}. The MS has the sensitivity to detect compounds and gases in Parts per billion (ppb), which was ensured with a quadrupole detection system, including a closed ion source, a triple mass filter and a dual (Faraday and Secondary Electron Multiplier) detector system. The weight of the sample used for the analysis was less than 2 mg. The ^1H and ^{13}C NMR measurements were performed by employing an Avance III HD spectrometer (Bruker, USA) at 400 MHz (^1H) and a broadband probe (PA BBO 400 MHz, Bruker). Solvent used is CD_3CN and $SiMe_4$ is used as the primary standard.

The ionic conductivity of XPE membranes and LiTFSI/PEGDME bulk solutions are determined by electrochemical impedance spectroscopy (EIS) analysis using an Autolab (PGSTAT204-FRA32M, Metrohm) potentiostat. In order to do this, the XPE is placed between two stainless steel blocking electrodes (area 1.54 cm^2) in a **2032-coin** cell assembly. Similarly, the Li-P-x solution soaked glass fiber separator (200 µl electrolyte, thickness 300 µm, diameter 18 mm) is assembled in between stainless steel current collectors of an EL-cell. The coin cells/EL-cells are assembled in a dry room. Prior to the EIS analysis, the cells are placed inside a climatic chamber (BINDER MK-53). The measurements were carried in the frequency range of 500 kHz to 1 Hz between 0°C and 70°C at

open circuit potential (OCP). The impedance responses are taken at every 10 °C interval by maintaining the temperature equilibrium for 2 h. In order to calculate the ionic conductivity (σ, Scm^{-1}) the Equation S1 is used, where 'R_b' is the bulk resistance, '*l*' is the thickness, and '*A*' is the area of the sample.

$$\boldsymbol{\sigma = lA^{-1}R_b^{-1}} \qquad \text{(Equation S1)}$$

The ionic conductivity values obtained at various temperatures are fitted with Vogel–Tamman–Fulcher (VTF) equation (Equation S2). The VTF equation represents the relationship between viscosity and temperature near T_g of the polymer matrix. The Equation S2is given below:

$$\boldsymbol{\sigma = A\exp\left(-\frac{Ea}{R(T-To)}\right)} \qquad \text{(Equation S2)}$$

Where A is the pre-exponential factor related to charge carrier concentration, '*σ*' is the ionic conductivity, 'E_a' is the activation energy (E_a^{VTF}), '*R*' is the gas constant, '*T*' is the experimental temperature and 'T_0'is the temperature which is 50 °C below the T_g.

The salt diffusion coefficient of the XPE membranes (D_{Li^+}) is estimated using the method reported by Ma *et al.* In this work, the XPE sandwiched lithium symmetrical cells are polarized at 20 mV for 1 h. followed by keeping the cell at OCP until a stable state is achieved. Later, from the plot of natural logarithm of potential (V) *vs*. time (t), the D_{Li^+} values were calculated using the following Equation S3:

$$\boldsymbol{Slope = (\pi^2 D_{Li+})L^{-2}} \qquad \text{(Equation S3)}$$

Where the slope is obtained by the linear fitting of the plot of -ln (V) *vs*. t, '*L*' is the thickness of the XPE specimen under consideration.

The Li-ion transference number (T_{Li^+}) of the XPEs are measured at 60°C by using combined AC impedance spectroscopy and DC polarization measurements using Equation S4.

$$\boldsymbol{T_{Li^+} = \frac{I_S R_S(\Delta V - I_0 R_{ct,0})}{I_0 R_{\Omega,0}(\Delta V - I_S R_{ct,S})}} \qquad \text{(Equation S4)}$$

Here, *V* is the DC polarization voltage (10 mV), $\boldsymbol{I_0}$ and $\boldsymbol{I_S}$ are the initial and steady-state current responses during the DC polarization, $\boldsymbol{R_0}$ and $\boldsymbol{R_{ct,0}}$ stand for the bulk resistance and charge transfer resistance, respectively, which is obtained from the Nyquist plot prior to the DC polarization. Similarly, $\boldsymbol{R_s}$ and $\boldsymbol{R_{ct,s}}$ stand for the bulk and charge transfer resistance obtained after achieving steady-state conditions.

The oxidation stability (anodic stability) of the XPE was evaluated by linear sweep voltammetry (LSV), and the reduction stability (cathodic stability) by employing cyclic voltammetry (CV) using a potentiostat (VMP3, Bio-logic, Switzerland). In both measurements, a scan rate of 0.1 $mVs^{-1}$was employed. The LSV tests are run between OCP and 7 V vs. $Li|Li^+$, where aluminum (Al) or stainless steel (StSt) is used as the working electrode (Li|XPE|Al or Li|XPE|SS). A limiting current of 1 µA cm^{-2} is considered as the onset of decomposition process and corresponding voltage is considered as the maximum application voltage in the case of LSV measurements. Similarly, the CV is carried out between OCP and -0.25V vs. $Li|Li^+$ with copper (Cu) as the working electrode (Li|XPE|Cu). In both cases, lithium is used as a reference electrode. Galvanostatic lithium plating/stripping measurements are carried out in a symmetric cell configuration *viz*., Li|XPE|Li. Measurements are carried out at 60°C at a current density of 0.1 mA cm^{-2}(5h Li-plating and 5h Li-stripping).

Fabrication of electrodes and electrochemical characterization

Lab scale lithium metal cells are prepared using C-$LiFePO_4$ or $Li[Ni_{0.8}Co_{0.15}Al_{0.05}]O_2$ as a cathode, lithium metal as an anode and the XPE membranes as separator and electrolyte. A typical cathode is composed of active material, PVdF as binder and Super P carbon as conductive additive. An NMP based slurry consisting of active material, PVdF and SuperP in 90:5:5 ratios are prepared. This slurry is then cast on to an aluminum foil and dried at 60°C overnight. Later, the electrodes were cut into a disk of 14 mm diameter and dried at 120°C under high vacuum for 12 h. The mass loading of $LiFePO_4$ electrode is 3 mg cm^{-2} whereas the electrode prepared with $Li[Ni_{0.8}Co_{0.15}Al_{0.05}]O_2$ has a mass loading of 1.5 $mgcm^{-2}$. Coin cells of 2032 type are prepared in the dry room using the cell components, and their electrochemical characteristics were investigated at 20, 40 and 60°C in terms of constant current charge/discharge cycling at different current intensities using a MACCOR cycler (Series 4000). The galvanostatic charge-discharge studies were carried out in the range of 2.5 - 4 V vs. $Li|Li^+$ for $LiFePO_4$ and 2.7-4.3 V *vs*. $Li|Li^+$ for $Li[Ni_{0.8}Co_{0.15}Al_{0.05}]O_2$. Prior to cycling, all cells were equilibrated to 60°C.

Quantum chemistry calculations

Intrinsic oxidative stabilities have been computed for PEGDME and various clusters involving PEGDME and Li^+. The calculations have been performed with the Gaussian 16 package[6] at different levels of theory: For larger complexes involving a single PEGDME chain with monomers and multiple lithium ions, both the semi-empirical PM6 method[7] and density functional theory (DFT) with the range-separated LC-ωPBE functional[8]have been used in combination with the 6-31+G(d,p) basis set. All calculations have been performed using the SMD implicit solvation model[9] with the parameters for "ether" contained in Gaussian 16. The oxidation potentials E_{ox} have been computed via the following equation[10],

$$\boldsymbol{E}_{\mathrm{ox}} = \frac{\boldsymbol{G}(\boldsymbol{M}^+) - \boldsymbol{G}(\boldsymbol{M})}{\boldsymbol{F}} - \mathbf{1.4}\ \boldsymbol{V} \qquad \text{(Equation S5)}$$

Where, $G(M)$ and $G(M^+)$ are the computed free energies of the non-oxidized and the oxidized molecule or cluster, respectively, F is the Faraday constant, and the shift of 1.4 V relates the absolute free energy differences to the $Li|Li^+$ scale.[10,11]The geometry of the oxidized cluster has been re-optimized such that the potentials correspond to adiabatic potentials.[10]To validate the semi-empirical PM6 method and the LC-ωPBE function required to computationally tackle the larger clusters, additional calculations with the highly accurate but demanding G4MP2 method[12] have been carried out for a PEGDME-Li^+ complex with monomers and a single lithium ion. While G4MP2 yields E_{ox} = 6.7 V vs. $Li|Li^+$, values of 6.4 V vs. $Li|Li^+$ and 7.0 V vs. $Li|Li^+$ are obtained at the PM6 and LC-ωPBE/6-31+G(d,p) level, respectively. Although the absolute deviations are in the range of 0.3 V, we therefore have confidence that both computationally expedient methods yield satisfactory results.

SI Section 2: NMR Spectra

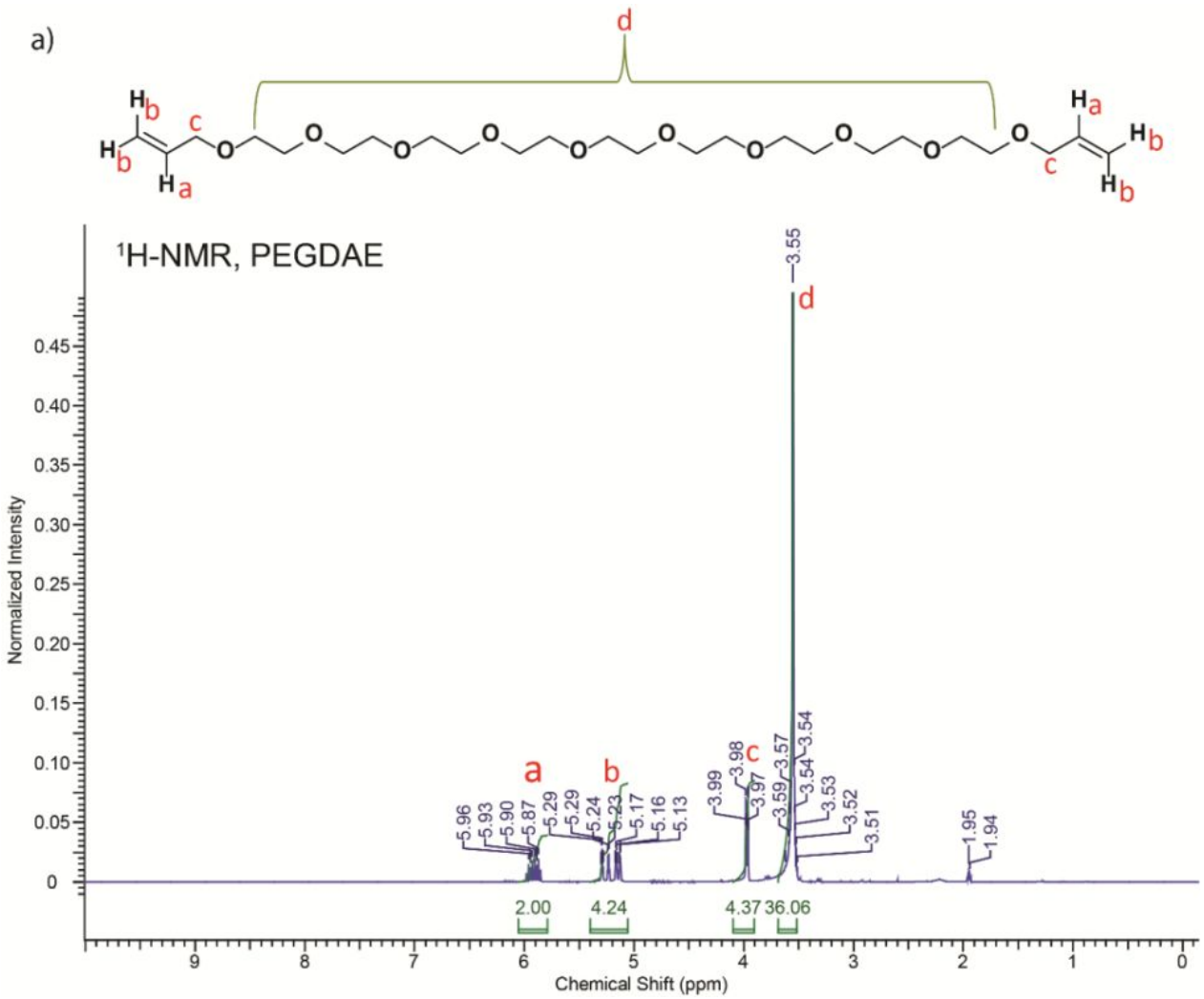

Figure S1 a) ^{1}H-NMR spectrum of the oligomer cross-linker PEGDAE.

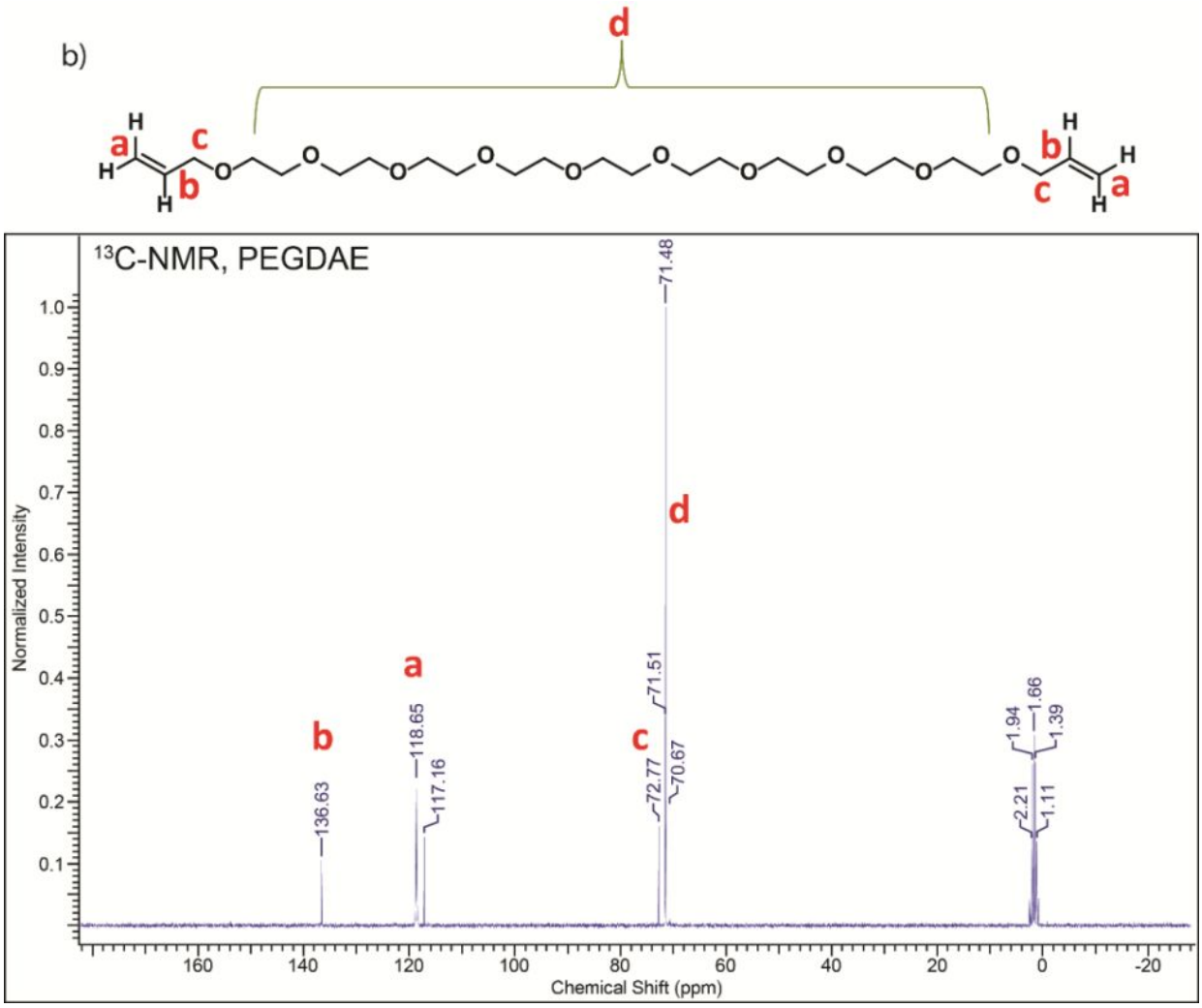

Figure S1b)^{13}C-NMR spectrum of the cross-linker monomer PEGDAE.

From the ^{1}H-NMR spectra, the formation of PEGDAE is confirmed. The absence of peaks corresponding to any trace impurities underlines that PEGDAE is obtained in its purest form. Additionally, in the ^{1}H-NMR spectrum, peaks corresponding to -OH group is also absent further evidencing the complete conversion of PEG to PEGDAE. For instance, the peaks observed between 5.87-5.96 (m), 5.13-5.29 (m) and 3.97-3.99 ppm (m) are related to the protons from the terminal allyl ether groups (-OCH_2-CH=CH_2). At the same time, the broad peaks between 3.51-3.59 ppm correspond to the remaining 36 protons present in the ethylene oxide (-EO) units in PEGDAE. The ^{13}C-NMR spectrum also supports the structure elucidated from^{1}H-NMR spectrum.

SI Section 3: Structure and mechanical stability of XPE

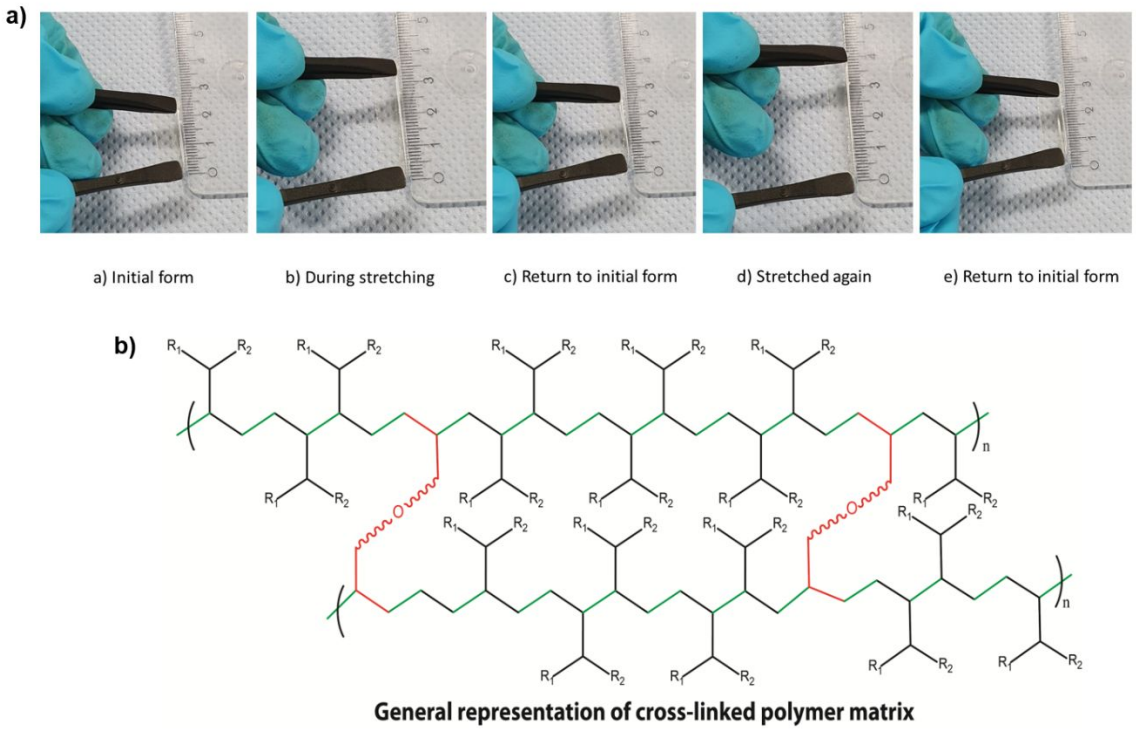

Figure S2 a) Digital images representing the mechanical stability of D-XPE-2 membranes under repeated stretching conditions b) General representation of a cross-linked polymer network.

SI Section 4: ATR-FTIR Spectra

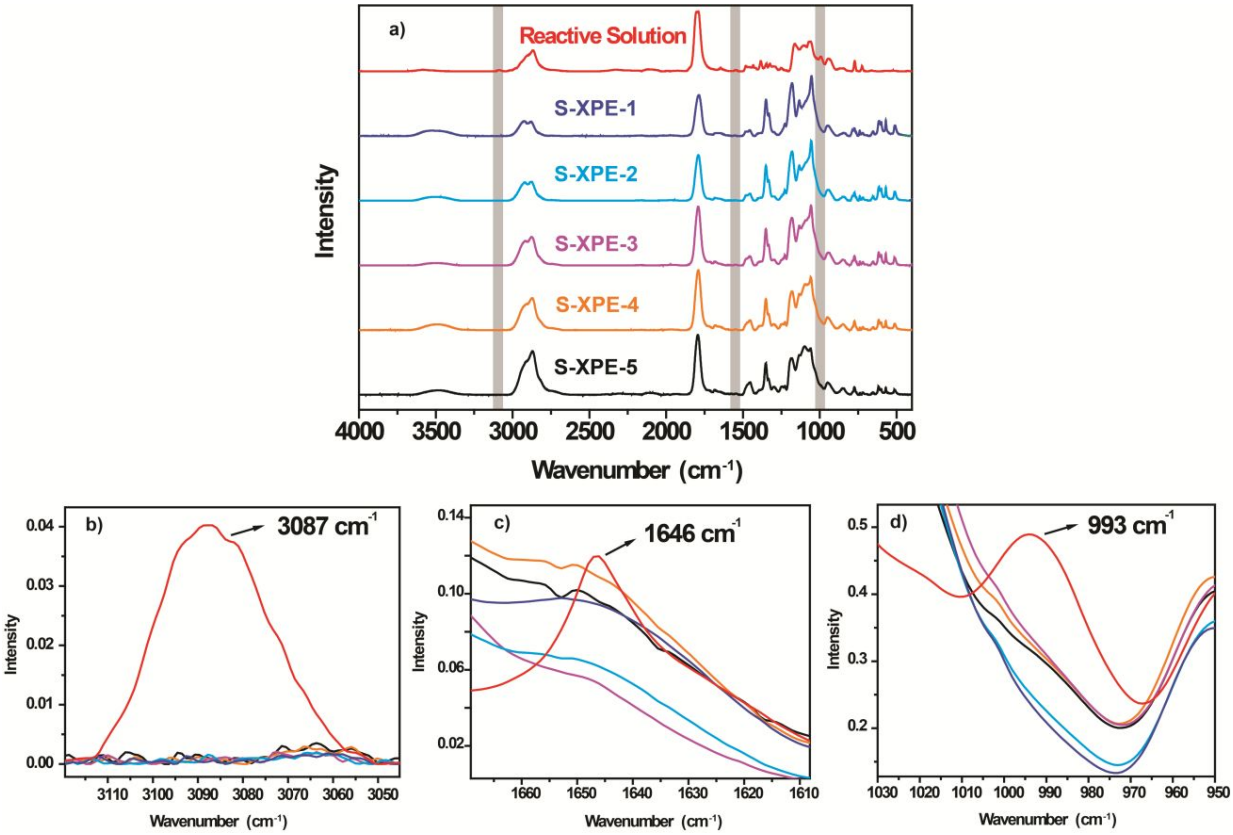

Figure S3 ATR-FTIR spectra of the reactive solution and the S-XPE-x samples from a) 400 to 4000 cm^{-1}. The magnified spectra in the wavenumber regions of b) 3045-3120 cm^{-1}, c) 1605-1670 cm^{-1}, and d) 950-1030 cm^{-1}, representing the disappearance of the peaks corresponding to-C=C- bonds.

Sample	Peak position (cm^{-1})			T_g (°C)
	L_P	M_P	R_P	
Li-P-1	1133	1098	1059	-67
Li-P-2	1133	1094	1058	-68
Li-P-3	1133	1093	1056	-59
Li-P-4	1134	1092	1057	-46
Li-P-5	1133	1091	1058	-30

Table S4 The changes associated with the L_P, M_P and R_P peak positions of the entire Li-P-x samples and their respective T_g values.

The single peak at 1098 cm^{-1} in between the wavelength region of 1040-1160 cm^{-1} as observed in the case of PEGDME is subjected to tremendous changes with the addition of LiTFSI into it. With the addition of LiTFSI into PEGDME (Li-P-1), a set of two new shoulder peaks are appeared neighboring the broad M_P peak at 1098 cm^{-1}. These triplet peaks are positioned at 1133 cm^{-1} (L_P), 1098 cm^{-1} (M_P) and 1059 cm^{-1} (R_P), respectively. The observation of triplet peak is associated with the conformational changes occurred in PEGDME as already explained in the main text (**Section 2.2**). From, the nature of these triplet peaks, it is possible to decipher the interaction of Li^+ ions with –EO units and the accompanied conformational changes occurred in the system. The subsequent addition of LiTFSI into PEGDME is accompanied with apparent changes in the position and intensity of L_P, M_P and R_P peaks. The changes associated with the peak positions of all Li-P-x samples are summarized in **Table S4**. The redshift observed for M_P peak as we move from Li-P-1 to Li-P-5, and R_p peak from Li-P-1 to Li-P-3 indicate an enhanced interaction between oxygen atom of -EO units and Li^+-ions at high salt concentrations. However, in the case of Li-P-4 and Li-P-5 samples, the effect is reversed in such a way that the R_p peaks are observed at higher wavenumber values viz., 1057 and 1058 cm^{-1}, respectively. The observed blueshift compared to Li-P-3 may be associated with the reduced interaction between Li^+-ions and –EO units as a result of the formation of ion-pair aggregates/ion clustering at very high salt content.[1]

Apart from the peak positions, the intensity of M_P and R_P peaks in each of the Li-P-x samples can also give valuable information regarding the interaction between -EO and Li^+-ions. As it can be seen from **Figure 2b** in main text, the intensity of the M_P peak is decreased with successive addition of LiTFSI into PEGDME. At the same time, the R_P peaks are sharp and more or less of the same intensity except for Li-P-1 sample. The reduction in the M_P peak intensity is associated with the decreased amount of free –EO units in the respective samples owing to the concomitant enhancement in the coordination of more –EO units with Li^+ ions. The evolution of sharp R_P peaks in the case of Li-P-2 to Li-P-5 samples compared to Li-P-1 is directly related to the reduction in M_P peak intensity, where the intensity of R_P peak corresponds to the amount of interacting –EO units.

Sample	Peak position (cm^{-1})			T_g(°C)
	L_{SX}	M_{SX}	R_{SX}	
S-XPE-1	1133	1098	1059	-54
S-XPE-2	1133	1094	1056	-52
S-XPE-3	1133	1093	1054	-41
S-XPE-4	1133	1093	1054	-30
S-XPE-5	1133	1093	1053	-24

Table S5 The changes associated with the L_{SX}, M_{SX} and R_{SX} peak positions of the entire series of S-XPE-x samples and their respective T_g values.

In the region between 1040 and 1160 cm^{-1}, the ATR-FTIR spectrum of the cross-linker (PEGDAE, **Figure 2c, Main text**) looks similar to that of PEGDME with a broad peak centered at 1098 cm^{-1}.This is obvious considering the structural similarity of both molecules except at their terminals. Interestingly, in the case of S-XPE-0, a broad triplet is observed with peak maximums at 1144 (L_{SX}), 1098 (M_{SX}) and 1060 cm^{-1} (R_{SX}), respectively. This is already explained in the main text by means of the chemical cross-links induced by X-PEGDAE. The triplet peaks are retained with the introduction of LiTFSI to form the XPEs. In the case of S-XPE-1 and -2, the intensity of the triplet peak is rather high compared to S-XPE-3,4 and 5.

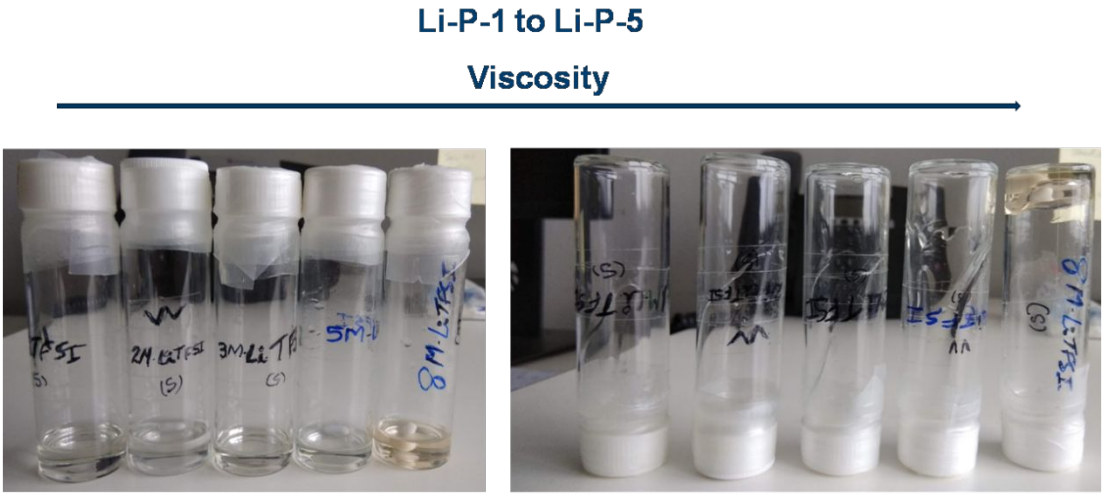

Figure S4 Digital images of the inversion tests of Li-P-X specimens showing the increment in viscosity with respect to an increase of LiTFSI content in PEGDME.

SI Section 5: Thermal characterization

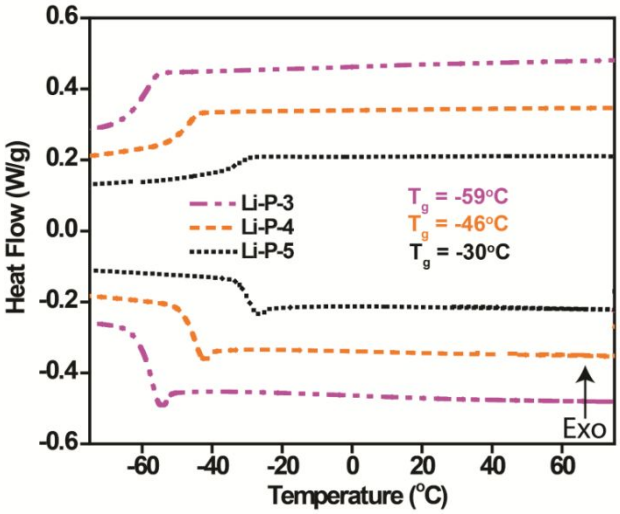

Figure S5 DSC thermograms ofLi-P-1, Li-P-2 and Li-P-3 solutions.

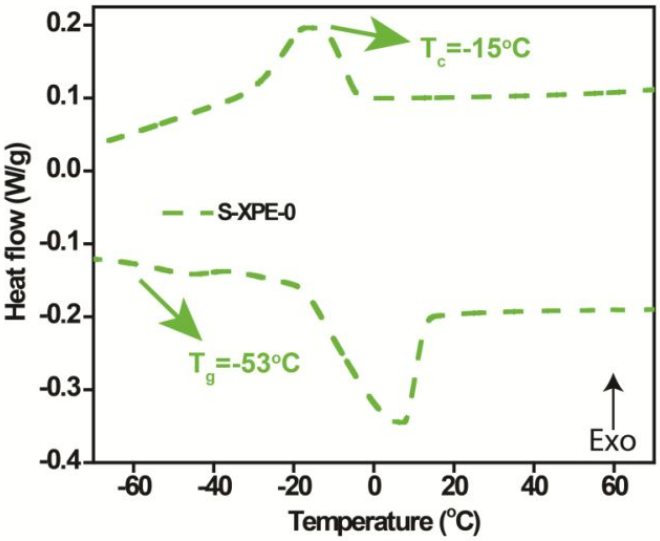

Figure S6 DSC thermograms of S-XPE-0 sample.

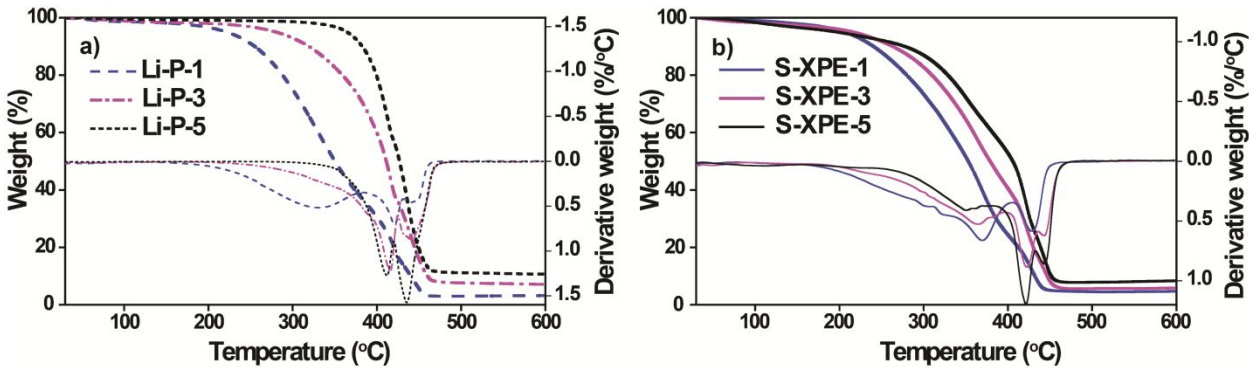

Figure S7a)TGA profiles of Li-P-x (x=1,3 and 5), and b) S-XPE-x (x=1, 3 and 5) samples.

The thermal stability of the Li-P-x and S-XPE-x samples is characterized by TGA analysis and the profiles are presented in **Figures S7a** and **b**, respectively. In the case of Li-P-1, three major weight lose regions are clearly observed. It can be seen from the derivative plot that the broad weight lose occurred in the region between 180-380°C correspond to the evaporation/degradation of PEGDME molecules present in Li-P-1.[2] The inflection point associated with this process is recorded to be at 329°C. Interestingly, in the case of Li-P-3, the degradation associated with PEGDME molecule is suppressed whereas the peak is completely disappeared in Li-P-5 sample. In other words, the onset of thermal degradation at 180°C in the case of Li-P-1 is significantly improved to about 300°C in the case of Li-P-5. This proves the favorable effect of higher salt content in improving the thermal stability of the Li-P-x samples. This further supports the claims regarding the changes in physiochemical properties of PEGDME by means of the interactions with Li^+-ions. The peaks beyond 400°C in the case of Li-P-x specimens are associated with the decomposition of LiTFSI.[3] In the case of S-XPE-x samples, the degradation peaks corresponding to the PEGDME molecules are not very prominent. However, considering the onset of degradation at 180°C similar to the case of Li-P-1, it can be concluded that PEGDME degradation is occurring in the case of S-XPE-1 as well. In the case of S-XPE samples also, the onset of PEGDME degradation is found to be increased with an increase in LiTFSI content. Hence, the maximum thermal stability is exhibited by S-XPE-5 which is up to 250°C. This value is 50°C less than the thermal stability of Li-P-5 sample and could be contributed from the degradation of the cross-linked polymer matrix, which is coupled with degradation of PEGDME. Additionally, an inflection point at 368°C is observed in the case of S-XPE-1 which could be due to the degradation of poly vinyl ethylene carbonate chains present in the cross-linked polymer matrix.[4,5] In the case of S-XPE-x specimens also, the weight loses beyond 400°C are attributed to LiTFSI decomposition. In both cases, as evidenced from MS spectra, water is expelled until 130°C for both Li-P-1 and S-XPE-1. Water was also evaporated from the system above 330°C due to the decomposition of ether molecules. Small amount of hydrocarbons are also escaped from both the samples only above 300°C. The main decomposition products of LiTFSI salt were the fluorinated carbons such as CF_3, and CF_2 at respective AMUs above 300°C. Thus, it can be concluded that the TGA results obtained are in agreement with the MS data with respect to assigning the stages of the sample decomposition.

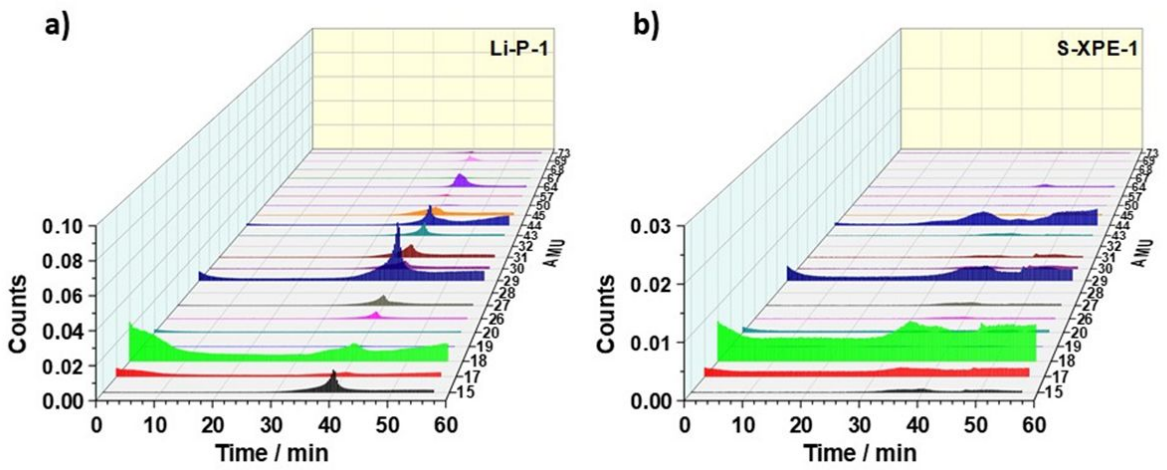

Figure S8 AMU of the products released during the TGA–MS analysis. The graph is reported as the ion current *vs.* test time for different molecules expelled during the TGA analysis of a) Li-P-1 salt, and b) S-XPE-1.

SI Section 6: Ionic Conductivity, activation energy and ESW of Li-P-x and D-XPE-x samples

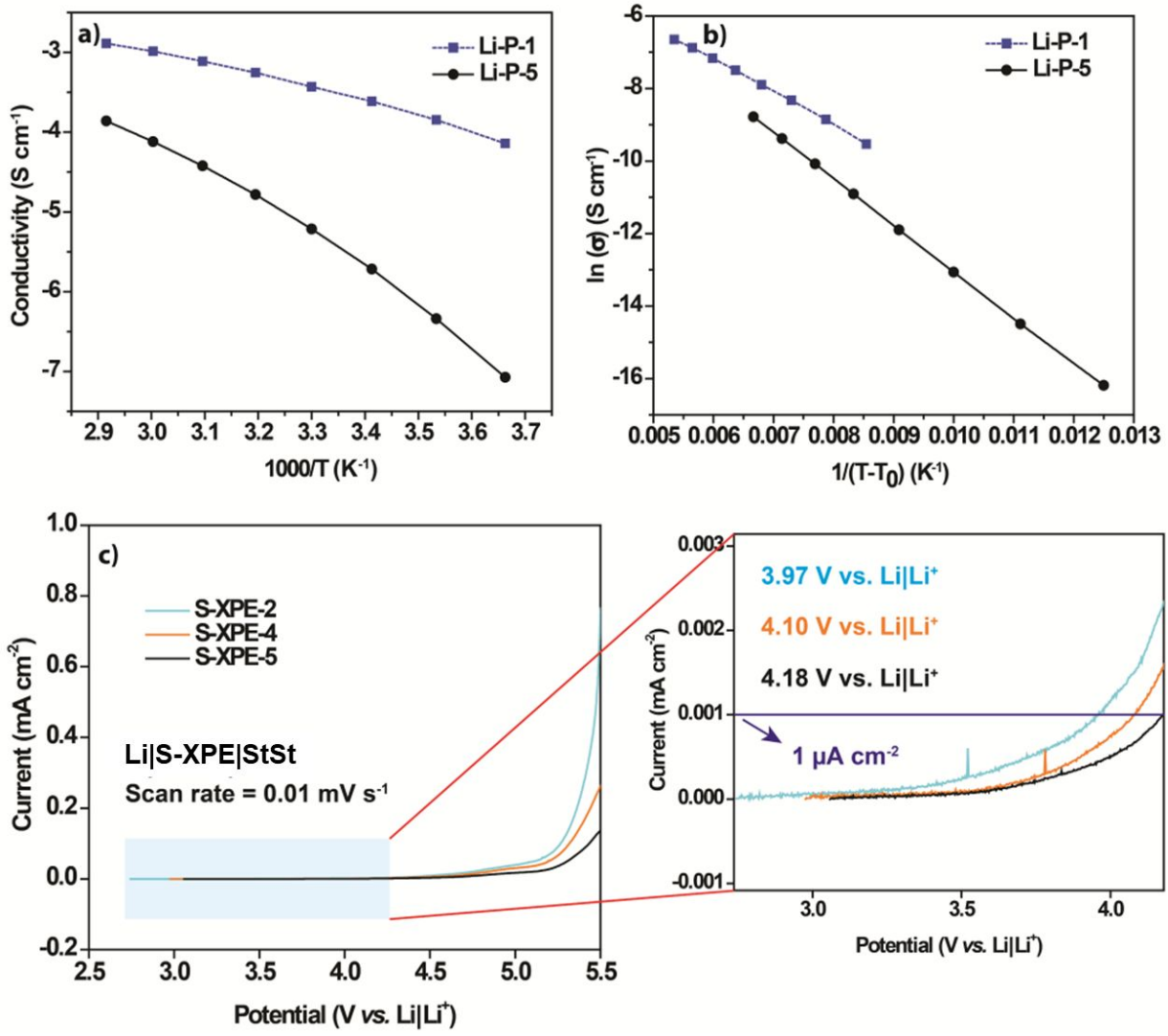

Figure S9 a) Ionic conductivity *vs*. temperature plot of the Li-P-1 and -5 samples, b) VTF fit of the same plot of Figure S9a, and c) determination of anodic stability of S-XPE-x membranes against stainless steel (StSt) as the working electrode.

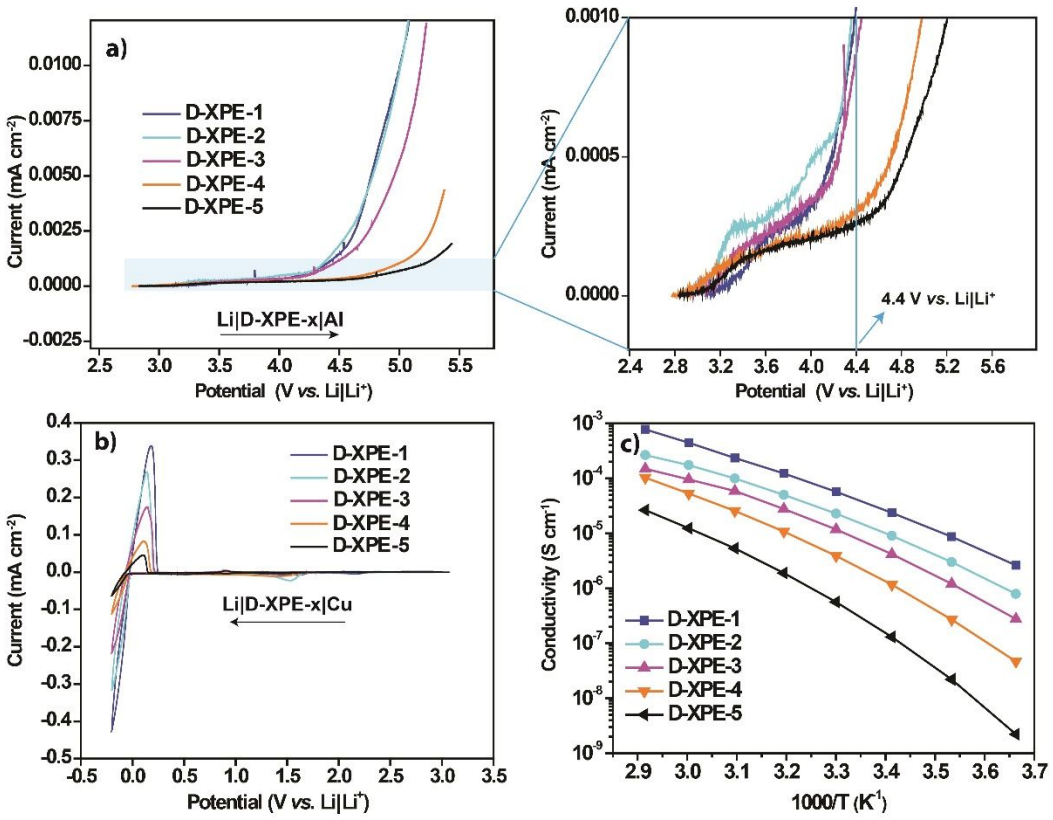

Figure S10 a) Current *vs*. potential (*vs*. Li|Li$^+$) plot representing the anodic stability of D-XPE-x samples, b) current *vs*. potential (*vs*. Li|Li$^+$) plot representing the cathodic stability of D-XPE-x samples, and c) the plot representing the change in ionic conductivity of D-XPE-x specimen with respect to temperature.

Sample	Ionic Conductivity (mS cm^{-1})		Transference No. (T_{Li^+})	Anodic stability (vs. Li|Li$^+$)
	30^{o}C	60^{o}C		
D-XPE-1	0.06	0.44	0.31	4.4
D-XPE-2	0.023	0.17	0.26	4.4
D-XPE-3	0.012	0.095	0.19	4.5
D-XPE-4	0.004	0.06	0.14	5
D-XPE-5	0.0006	0.012	0.11	5.2

Table S6 Ionic conductivity and anodic stability values of entire series of D-XPE-x specimens.

SI Section 7: Li plating/stripping and LMB characterization

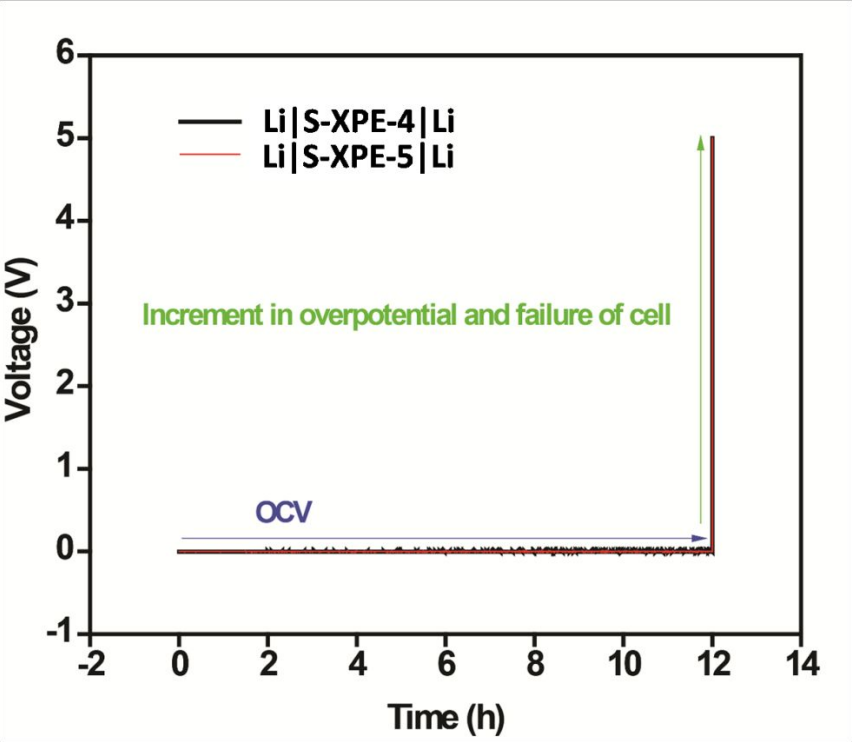

Figure S11 The plating/stripping profile of Li|S-XPE-4|Li and Li|S-XPE-5|Li cells.

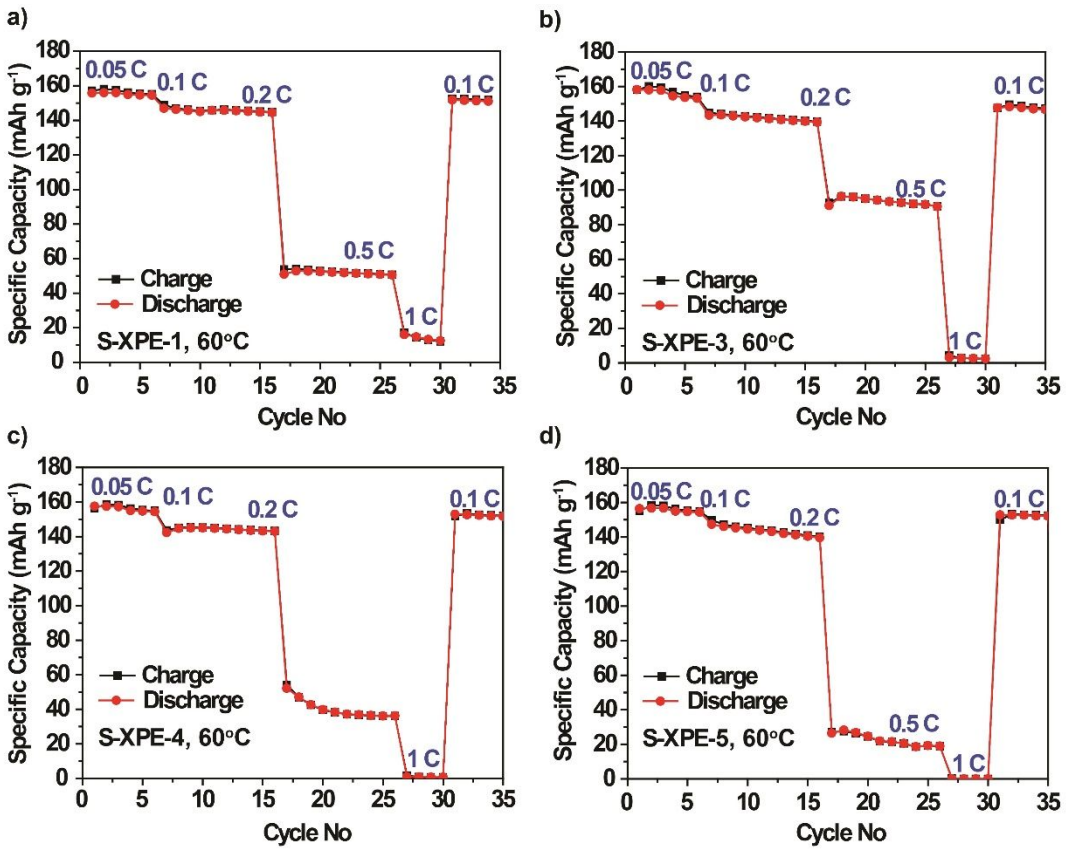

Figure S12 Specific capacity vs. cycle number plot corresponding to the a) LFP|S-XPE-1|Li b) LFP|S-XPE-3|Li c) LFP|S-XPE-4|Li d) LFP|S-XPE-5|Li cells at various C-rates (at 60°C).

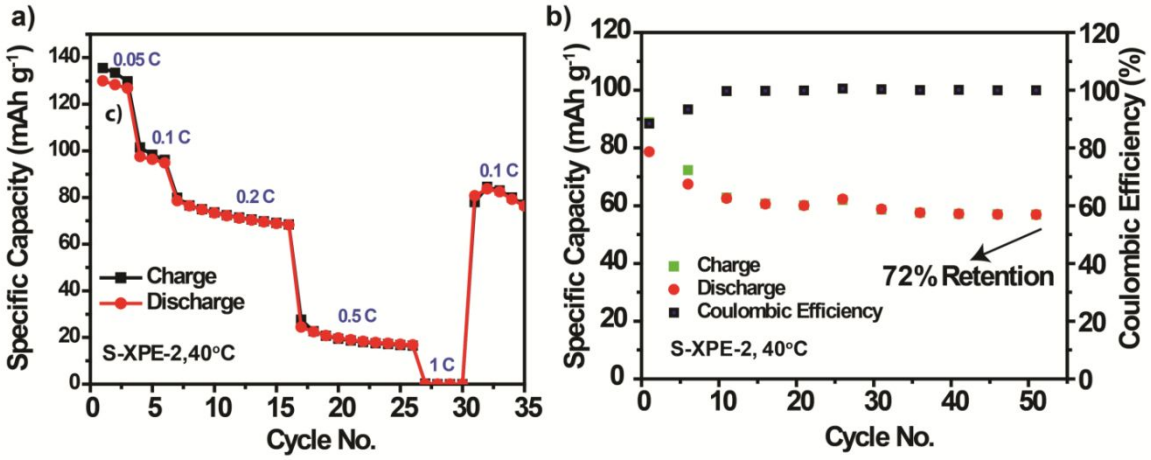

Figure S13 a) Specific capacity vs. cycle number plots corresponding to the LFP|S-XPE-2|Li cell at various C-rates (40°C) and b) long-term cycling stability ofLFP|S-XPE-2|Li cell at 0.2C and 40°C.

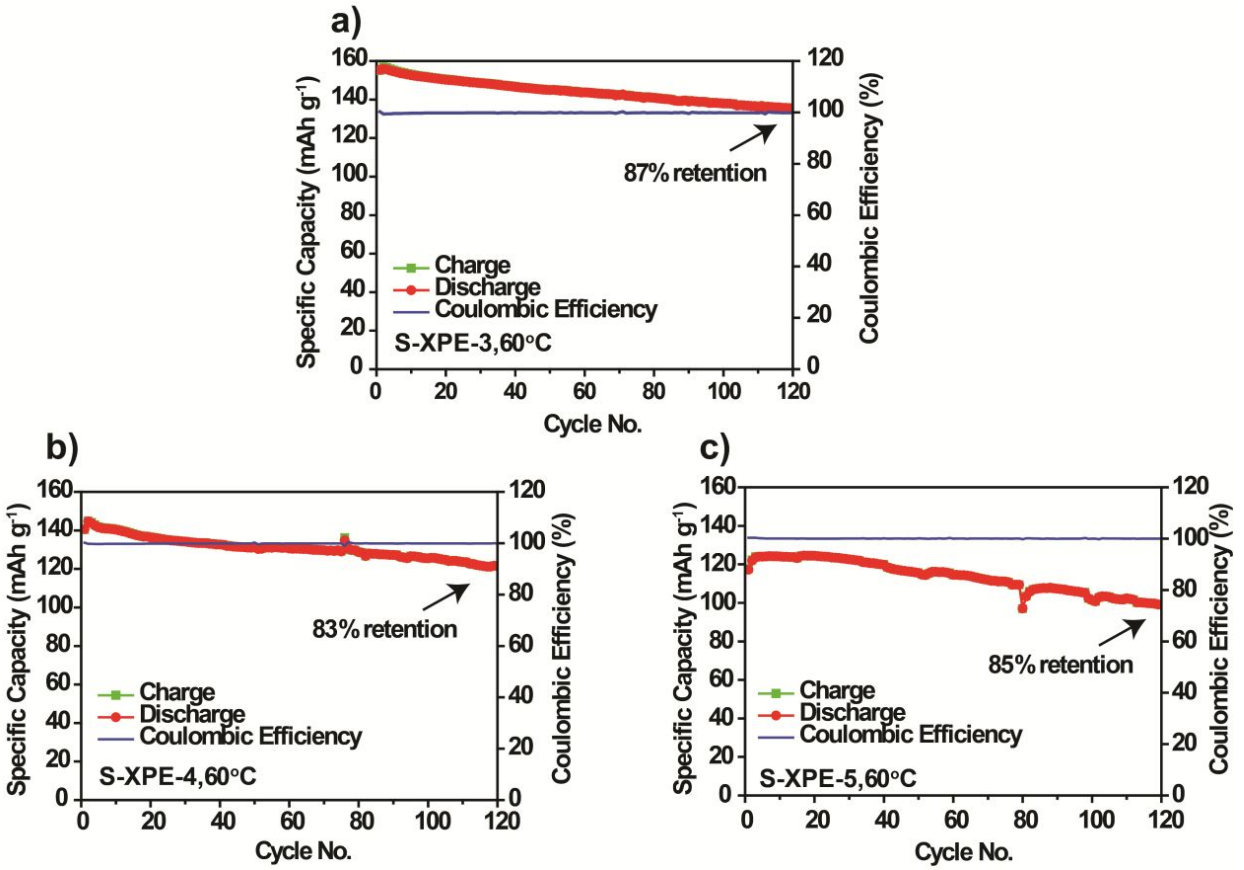

Figure S14 a) Long-term cycling stability of a) LFP|S-XPE-3|Li, b) LFP|S-XPE-3|Li and c) LFP|S-XPE-5|Li cells at 0.2C and 60°C.

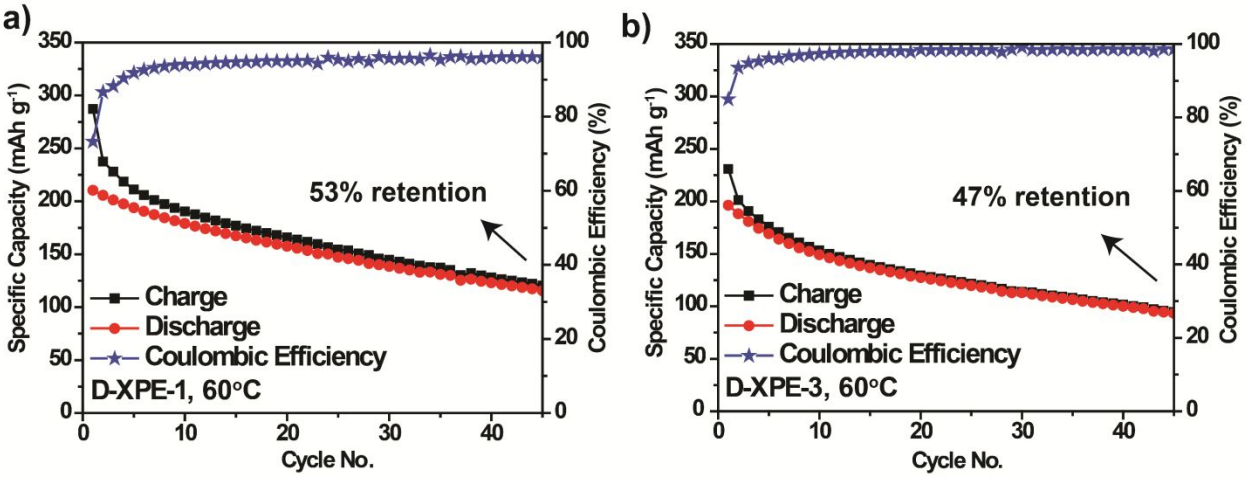

Figure S15 Long-term cycling stability of a) NCA|D-XPE-1|Li, and b) NCA|D-XPE-3|Li at 0.1C and 60°C.

References

1. N. Molinari, J. Mailoa and B. Kozinsky, *Chemistry of Materials*, 2018, **30**, 6298-6306.
2. L. Porcarelli, C. Gerbaldi, F. Bella and J. R. Nair*, Scientific Reports*, 2016, **6**, 19892.
3. R. He, M. Echeverri, D. Ward, Y. Zhu and T. Kyu, *Journal of Membrane Science*, 2016, **498**, 208-217.
4. J. Chai, Z. Liu, J. Zhang, J. Sun, Z. Tian, Y. Ji, K. Tang, X. Zhou and G. Cui, *ACS Applied Materials & Interfaces*, 2017, **9**, 17897-17905.
5. Y. Yoshida and T. Endo, *Polymer*, 2016, **102**, 167-175.
6. M. J.Frisch, G. W.Trucks, H. B.Schlegel, G. E.Scuseria, M. A.Robb, J. R.Cheeseman, G. Scalmani, V. Barone, G.A.Petersson, H.Nakatsuji, X. Li, M. Caricato, A. Marenich, J.Bloino, B. Janesko, R. Gomperts, B.Mennucci, H.P. Hratchian, J. V. Ortiz, A. F.Izmaylov, J. L.Sonnenberg, F. Ding, F. Lipparini, F.Egidi, J. Goings, B. Peng, A. Petrone, T. Henderson, D.Ranasinghe, V.G.Zakrzewski, J. Gao, N. Rega, Y. Honda, O. Kitao, H. Nakai, T. Vreven, K. Throssell, Jr. J.A. Montgomery. J. Peralta, F. Ogliaro, M.J. Bearpark, J.J.Heyd, E.N. Brothers, K.N. Kudin, V.N. Staroverov, T.A. Keith, R. Kobayashi, J. Normand, K.Raghavachari, A.P. Rendell, J.C. Burant, S.S.Iyengar, J. Tomasi, M.Cossi, J.M. Millam, M.Klene, C. Adamo, R.Cammi, J.W.Ochterski, R.L. Martin, K.Morokuma, O.Farkas, J.B.Foresman, D.J. Fox, Gaussian 16 Rev. B.01, Wallingford, CT, 2016.
7. J. Stewart, *Journal of Molecular Modeling*, 2007, **13**, 1173-1213.
8. O. Vydrov and G. Scuseria, *The Journal of Chemical Physics*, 2006, **125**, 234109.
9. Marenich, A. V.; Cramer, C. J.; Truhlar, D. G., J. Phys. Chem. B 2009, **113 (18)**, 6378-6396
10. O. Borodin, M. Olguin, C. Spear, K. Leiter and J. Knap, *Nanotechnology*, 2015, **26**, 354003.
11. O. Borodin, X. Ren, J. Vatamanu, A. von Wald Cresce, J. Knap and K. Xu, *Accounts of Chemical Research*, 2017, **50**, 2886-2894.
12. L. Curtiss, P. Redfern and K. Raghavachari, *The Journal of Chemical Physics*, 2007, **127**, 124105.